IEEE Access
Multidisciplinary | Rapid Review | Open Access Journal

Received June 10, 2020, accepted June 17, 2020, date of publication June 19, 2020, date of current version July 2, 2020.

Digital Object Identifier 10.1109/ACCESS.2020.3003794

A Novel Calculation Method to Design Parasitic Decoupling Technique for Two Antennas

MIN LI[1], (Member, IEEE), DI WU[2], (Member, IEEE), BING XIAO[1], (Student Member, IEEE), KWAN LAWRENCE YEUNG[1], (Senior Member, IEEE), AND LIJUN JIANG[1], (Fellow, IEEE)

[1]Department of Electrical and Electronic Engineering, The University of Hong Kong, Hong Kong
[2]College of Electronics and Information Engineering, Shenzhen University, Shenzhen 518060, China

Corresponding authors: Min Li (minli@eee.hku.hk) and Lijun Jiang (jianglj@hku.hk)

This work was supported in part by the Research Grants Council of Hong Kong under Grant GRF 17209918, Grant GRF 17207114, and Grant GRF 17210815, in part by the Asian Office of Aerospace Research and Development under Grant FA2386-17-1-0010, in part by the National Natural Science Foundation under Grant 61271158, in part by The University of Hong Kong Seed Fund under Grant 104005008, and in part by the Hong Kong University Grants Committee under Grant AoE/P-04/08.

ABSTRACT In this paper, a systematic and calculation-based parasitic decoupling technique (PDT) is proposed to mitigate the mutual coupling between two closely coupled antennas. The adopted parasitic decoupling structure consists of two transmission lines connected to the feed lines of antennas and a parasitic element connected with a transmission line and terminated by a reactive load. Rigorous decoupling theory and systematic design procedures are presented. The lengths of transmission lines and value of reactive load can be precisely calculated to increase antenna isolation. The superiority of the proposed PDT is verified by four decoupling examples. The simulated and measured results show that high isolations over 24 dB, efficiencies above 70%, and envelop correlation coefficients below 0.05 are achieved simultaneously. The results indicate the proposed PDT a promising decoupling method for MIMO systems.

INDEX TERMS Decoupling technique, high isolation, MIMO antenna, parasitic element, pattern diversity.

I. INTRODUCTION

In theory, the channel capacity of a multiple-input multiple-output (MIMO) system linearly increases with the increased channel number [1]. Nevertheless, for a size-constrained MIMO system having limited space for antennas, the channel capacity could be deteriorated by the mutual coupling among antenna elements. In the last few years, various decoupling techniques (DTs) have been presented to mitigate the above-mentioned antenna coupling [1]–[27], which can be roughly summarized into three categories of the inserted decoupling network scheme, the artificial metamaterial (MM) decoupling scheme, and the parasitic decoupling scheme.

1) The Inserted Decoupling Network Scheme [1]–[13]: Decoupling networks have many configurations such as the neutralization line, transmission line, reactive component, coupled-resonator, etc. Neutralization lines, as presented in [1]–[3], were connected with antenna radiators for isolation enhancement. However, the lack of a systematic approach to determine the location of the neutralization line makes this kind of DT heavily rely on the time-consuming optimization process. A decoupling feed network (DFN) is usually connected to antenna feed lines to increase port isolation [4]–[13]. In [4], authors proposed a simple DFN for two closely spaced antennas. By adding two transmission lines (TLs) to antennas' feed lines to realize an imaginary trans-admittance and utilizing a shunt reactive component attached in between the TL ends to cancel out the trans-admittance, the high port isolation, therefore, could be achieved. Based on this, several similar configurations were presented with the adopted reactive component in [4] being replaced by the synthesized microstrip lines [5], [6], lumped elements [7], decoupling and matching networks [8], [9], second-order coupled resonators [10]–[12], transmission-line network [13], etc. Notably, in [13], authors proposed to connect a transmission line with the reactive component in between two antennas' feed lines for isolation enhancement. It is effective for a MIMO array having two or three antenna elements. However, when the antenna number becomes larger, the implementation of DN becomes difficult due to the overlapping problem. Moreover, the DN is directly connected

The associate editor coordinating the review of this manuscript and approving it for publication was Walid Al-Hussaibi.

with the feed lines and so has a serious impact on matching conditions. As such, the realization of antenna matching after decoupling could be very difficult due to the complex DN for more antennas, even with the aid of matching networks. Additionally, regarding the DFNs in [4]–[13], optimizations for the network configuration were still necessary to achieve the good decoupling performances.

2) The Artificial MM Decoupling Scheme [14]–[21]: As common types of MMs, the electromagnetic band gap (EBG) structure and split ring resonator (SRR), have been widely used in MIMO system for antenna isolation. In [17], the EBG structures were integrated with antennas to suppress mutual coupling between two patches with an edge separation (edge-to-edge separation) of $0.75\lambda_0$. In [18], authors studied a uni-planar coupled EBG superstrate to reduce the coupling between two patches with a separation of $0.5\lambda_0$. The EBG-based DT is not appealing when the antenna separation is less than $0.5\lambda_0$, as the EBG structures are not small. Moreover, to realize the mushroom structure, the EBGs in [17] were embedded inside the substrate at the expense of increased fabrication complexity. In [19], the low-profile folded SRRs were employed on the ground plane for isolation improvement. A slot combined complementary SRR (SC-CSRR) structure was studied in [20] to reduce the coupling in a microstrip phased-array (MPA). However, the SRRs in [19], [20] resulted in the reductions of antenna gains and front-to-back ratios (FBRs). In [21], a modified SC-CSRR was printed on a superstrate of patch antennas to reduce the mutual coupling. The design maintained a high FBR, but the required edge separation is 3 times larger than that of [19]. Therefore, the MIMO designs employing artificial MM structures for isolation improvement suffer from either complicate fabrication process or negative impact on antenna radiation or large antenna separation.

3) The Parasitic Decoupling Scheme [22]–[27]: By incorporating with passive elements to produce the desired coupling against original coupling between antennas, high isolation can also be achieved. In [22], [23], the H-shaped, meandering T-shaped and U-shaped parasitic elements (PEs) were presented for decoupling dipoles, planar inverted F antennas (PIFAs) and patches, respectively, and parametrical sweeping was employed to design each structure. A canonical two-element MIMO slot antenna was presented in [24]. By incorporating with a coupling PE, the two-port antenna could achieve high port isolations. More importantly, by properly designing the PE and canonical two-port antenna, the coupling between two closely located canonical antennas could also be reduced, allowing them to be replicated and concatenated together to form a densely packed multi-element MIMO antenna. An array-antenna decoupling surface (ADS) was presented in [25]. The ADS can be regarded as a deformed PE that exhibits the advantage of applicability to large-scale arrays and drawback of resulting in high profile height. Both designs in [24], [25] achieved acceptable levels of antenna isolation but required specific optimizations for the PEs in [24] and the ADS in [25]. Another kind of parasitic decoupling solution was presented in [26], which utilized a reactively loaded PE in between antennas for isolation enhancement. Following this strategy, similar work for a symmetric four-element array was presented in [27]. Both designs achieved high port isolations but the dimensions of PE & antennas in [26] and the PE configuration & reactive-load value in [27] were required to be optimized for the high isolation. Therefore, regarding the existing literature on parasitic decoupling technique (PDT), the antennas or PEs need to be tuned through parameter sweep to meet each design requirement, which could be a labor-intensive process.

In this paper, we propose a systematic and calculation-based approach to design the PDT for closely coupled antennas, which is for the first time to propose a decoupling method using parasitic decoupling structure (PDS) without any parametrical optimization for the antenna or PE. Comparing with the existing decoupling solutions, the proposed PDT demonstrates the following attractive features.

1) Preciseness: The PDT has rigorous design formulas. All the parameter variables can be calculated to achieve high isolation, i.e., no parametrical optimization is needed.

2) Generality: The PDT has no limitations on antenna type or configuration.

3) Potential: Benefiting from the non-optimization characteristic, the PDT demonstrates the potential for multiple-element MIMO antennas.

The remaining part is organized as follows: Section II describes the decoupling methodology. Four detailed examples are presented and used to estimate the proposed PDT in Section III. Finally, conclusions are given in Section IV.

II. DECOUPLING METHODOLOGY

A. DERIVATION OF PARASITIC DECOUPLING REPRESENTATION

To decouple a two-element antenna array, a PE is inserted in between the antenna elements with its schematic shown in Fig. 1. Ant 1 and Ant 2 represent two radiating elements and the PE is a passive element terminated by a reactive load Z_{L1}. The adopted PDS consists of two transmission lines (TLs) with the same characteristic impedance Z_0 (normally equal to 50 Ω) and the electrical lengths θ_1 and θ_2 connected with antenna feed lines, and a PE connected with a TL (Z_0, θ_3) and terminated by a reactive load Z_{L1}.

As shown in Fig. 1, the scattering matrix of the three-port network of two antennas and one PE is denoted by $[S^{t1}]$ at the reference plane t_1. By introducing phase delays to the network through adding additional TLs individually to each feed line, a new scattering matrix $[S^{t2}]$ is resulted at the reference plane t_2. After terminating the PE by a reactive load Z_{L1}, the scattering matrix $[S^{t3}]$ of the decoupled antennas is obtained at the reference plane t_3. With adding a matching network at each antenna input, the scattering matrix $[S^{t4}]$ of the decoupled and matched antennas can be obtained at the reference plane t_4.

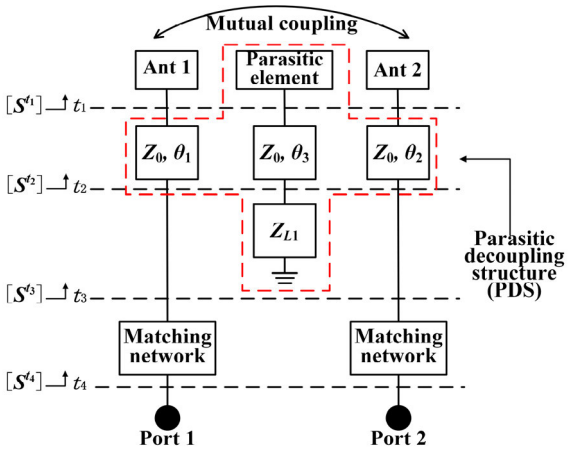

FIGURE 1. The configuration diagram of the proposed parasitic decoupling technique.

The MIMO system in Fig. 1 consists of two antennas and the proposed PDS, whose scattering matrix at a certain frequency f_0 can be expressed by a 3×3 matrix at the reference plane t_1, i.e.,

$$\mathbf{S^{t_1}} = \begin{bmatrix} \alpha_{A1A1} e^{j\phi_{A1A1}} & \alpha_{A1,A2} e^{j\phi_{A1A2}} & \alpha_{A1,P1} e^{j\phi_{A1P1}} \\ \alpha_{A2,A1} e^{j\phi_{A2A1}} & \alpha_{A2,A2} e^{j\phi_{A2A2}} & \alpha_{A2,P1} e^{j\phi_{A2P1}} \\ \alpha_{P1,A1} e^{j\phi_{P1A1}} & \alpha_{P1,A2} e^{j\phi_{P1A2}} & \alpha_{P1,P1} e^{j\phi_{P1P1}} \end{bmatrix}, \quad (1)$$

where A and P denote the antenna and PE ports, respectively.

After adding three TLs (Z_0, $\theta_1 - \theta_3$), the transmission and reflection coefficients perform additional phase delays, resulting in $[S^{t2}]$ at t_2 as (2), shown at the bottom of the next page.

The desired phase-delay values $\{\theta_i \in \boldsymbol{\theta}, i \in [1, 3]\}$ will be determined later. Applying an S-to-Z transformation [28] to (2) yields the impedance matrix $[Z^{t2}]$ as

$$\mathbf{Z^{t_2}} = Z_0 \left(\mathbf{U} + \mathbf{S^{t_2}}\right)\left(\mathbf{U} - \mathbf{S^{t_2}}\right)^{-1} = \begin{bmatrix} Z^{t_2}_{A1A1} & Z^{t_2}_{A1A2} & Z^{t_2}_{A1P1} \\ Z^{t_2}_{A2A1} & Z^{t_2}_{A2A2} & Z^{t_2}_{A2P1} \\ Z^{t_2}_{P1A1} & Z^{t_2}_{P1A2} & Z^{t_2}_{P1P1} \end{bmatrix} \quad (3)$$

Additionally, the voltage-current relation of the three-port network, as shown in Fig. 2(a), can be described by

$$\begin{bmatrix} V^{t_2}_{A1} \\ V^{t_2}_{A2} \\ V^{t_2}_{P1} \end{bmatrix} = \begin{bmatrix} Z^{t_2}_{A1A1} & Z^{t_2}_{A1A2} & Z^{t_2}_{A1P1} \\ Z^{t_2}_{A2A1} & Z^{t_2}_{A2A2} & Z^{t_2}_{A2P1} \\ Z^{t_2}_{P1A1} & Z^{t_2}_{P1A2} & Z^{t_2}_{P1P1} \end{bmatrix} \begin{bmatrix} I^{t_2}_{A1} \\ I^{t_2}_{A2} \\ I^{t_2}_{P1} \end{bmatrix}, \quad (4)$$

where $V^{t_2}_{Ai}$ and $I^{t_2}_{Ai}$, $\{i \in [1, 2]\}$, denote the voltage and current, respectively, at antenna port i, and $V^{t_2}_{P1}$ and $I^{t_2}_{P1}$ are the voltage and current, respectively, at the PE port. If the PE is terminated by a reactive load Z_{L1}, as shown in Fig. 2(b), the voltage-current relationship across the PE port can be described by

$$V^{t_2}_{P1} = -Z_{L1} I^{t_2}_{P1}. \quad (5)$$

Substituting (5) into (4), $\left\{V^{t_2}_{Ai}, i \in [1, 2]\right\}$ in (4) can be rewritten by a new set of equations. Rearranging these equations

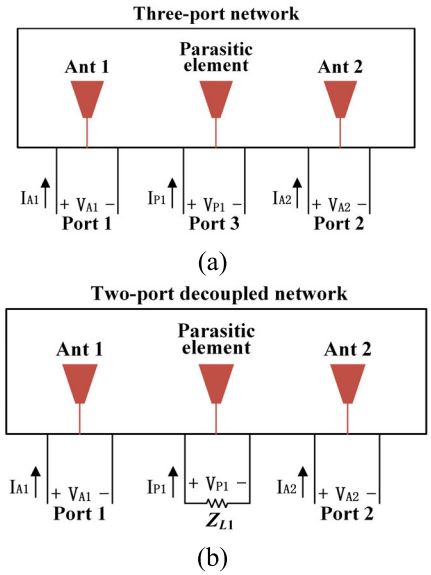

FIGURE 2. The voltage-current model. (a) Three-port network having two antennas and one PE. (b) Two-port network having the PE terminated by load Z_{L1}.

produces a new impedance matrix across antenna inputs at t_3 as:

$$\begin{bmatrix} V^{t_3}_{A1} \\ V^{t_3}_{A2} \end{bmatrix} = \begin{bmatrix} Z^{t_3}_{A1A1} & Z^{t_3}_{A1A2} \\ Z^{t_3}_{A2A1} & Z^{t_3}_{A2A2} \end{bmatrix} \begin{bmatrix} I^{t_3}_{A1} \\ I^{t_3}_{A2} \end{bmatrix}, \quad (6)$$

or $\mathbf{V^{t3}} = \mathbf{Z^{t3}} \mathbf{I^{t3}}$, where $[Z^{t3}]$ is readily shown as

$$\mathbf{Z^{t_3}} = \begin{bmatrix} Z^{t_2}_{A1A1} & Z^{t_2}_{A1A2} \\ Z^{t_2}_{A2A1} & Z^{t_2}_{A2A2} \end{bmatrix} - \frac{1}{Z^{t_2}_{P1P1} + Z_{L1}} \begin{bmatrix} Z^{t_2}_{A1P1} \\ Z^{t_2}_{A2P1} \end{bmatrix} \begin{bmatrix} Z^{t_2}_{P1A1} & Z^{t_2}_{P1A2} \end{bmatrix} \quad (7)$$

Applying a Z-to-S transformation [28] to (7), the scattering matrix $[S^{t3}]$ of the two antennas can be written as

$$\begin{aligned} \mathbf{S^{t_3}} &= \left(\mathbf{Z^{t_3}}/Z_0 + \mathbf{U}\right)^{-1} \left(\mathbf{Z^{t_3}}/Z_0 - \mathbf{U}\right) \\ &= \begin{bmatrix} f^{t_3}_{A1A1}(Z_{L1}, \boldsymbol{\theta}) & f^{t_3}_{A1A2}(Z_{L1}, \boldsymbol{\theta}) \\ f^{t_3}_{A2A1}(Z_{L1}, \boldsymbol{\theta}) & f^{t_3}_{A2A2}(Z_{L1}, \boldsymbol{\theta}) \end{bmatrix} \end{aligned} \quad (8)$$

where $\left\{f^{t_3}_{AiAj}(Z_{L1}, \boldsymbol{\theta}) \in \mathbf{S^{t_3}}, i, j \in [1, 2]\right\}$ have complex values and are functions of the phase-delay variables $\{\theta_i \in \boldsymbol{\theta}, i \in [1, 3]\}$ and load variable Z_{L1} introduced by PDS. The parameters $\left\{f^{t_3}_{AiAj}(Z_{L1}, \boldsymbol{\theta}) \in \mathbf{S^{t_3}}, i = j \in [1, 2]\right\}$ are reflection coefficients and indicate matching conditions at port i, and the parameters $\left\{f^{t_3}_{AiAj}(Z_{L1}, \boldsymbol{\theta}) \in \mathbf{S^{t_3}}, i \neq j \in [1, 2]\right\}$ represent coupling coefficients from port j to i and indicate the mutual coupling between ports i and j. Moreover, the reciprocity $S^{t_3}_{12} = S^{t_3}_{21}$ leads to $f^{t_3}_{A1A2} = f^{t_3}_{A2A1}$. To eliminate the mutual coupling, the decoupling condition is given as

$$S^{t_3}_{21} = f^{t_3}_{A2A1}(Z_{L1}, \boldsymbol{\theta}) = 0. \quad (9a)$$

Solving (9a) for Z_{L1} yields the following

$$Z_{L1} = \frac{Z^{t_2}_{A2P1} \cdot Z^{t_2}_{P1A1}}{Z^{t_2}_{A2A1}} - Z^{t_2}_{P1P1} = f_{Z_{L1}}\{\theta_i\}, \quad \{\theta_i \in \boldsymbol{\theta}, i \in [1, 3]\}. \tag{9b}$$

Additionally, higher radiation efficiency is always preferred for MIMO antennas. Hence, the real part in Z_{L1} representing resistance should be zero to circumvent the ohmic loss, i.e.,

$$\mathrm{Re}\{Z_{L1}\} = \mathrm{Re}\{f_{Z_{L1}}\{\theta_i\}\} = 0, \quad \{\theta_i \in \boldsymbol{\theta}, i \in [1, 3]\}. \tag{10}$$

So the phase-delay parameters $\boldsymbol{\theta}$ can be calculated by (10), which could have many solutions. The determined $\boldsymbol{\theta}$ is put back into (9b) to determine the reactance Z_{L1}. The reactive Z_{L1} can be appropriately realized by a capacitor or an inductor.

Besides, the Z_{L1} in (9b) that satisfies the decoupling condition of (9a) can be substituted into (7) to obtain the input impedances of the decoupled antennas as

$$Z^{t_3}_{A1A1} = Z^{t_2}_{A1A1} - \frac{Z^{t_2}_{A2A1} \cdot Z^{t_2}_{A1P1}}{Z^{t_2}_{A2P1}} \tag{11a}$$

$$Z^{t_3}_{A2A2} = Z^{t_2}_{A2A2} - \frac{Z^{t_2}_{A2A1} \cdot Z^{t_2}_{A2P1}}{Z^{t_2}_{A1P1}} \tag{11b}$$

The obtained impedances are used to design the matching circuits.

B. DESIGN PROCEDURE

Based on the above discussion, the design procedures are summarized as follows:

I. Design and implement a PE in between two coupled antennas and obtain $[S^{t1}]$ of the three-port network using measurement/simulation or any other methods. Two essential factors should be taken into account when designing the PE. 1) The resonant frequency of the PE should be close to that of the antennas so that the PE and antennas could have mutual coupling, although the PE could have a different size or shape or antenna type from the antenna. 2) The PE should be placed in the near-field region of the antennas to produce the desired interference.

II. Introduce phase delays $\boldsymbol{\theta}$ for the antennas & PE and obtain $[S^{t2}]$.

III. Terminate the PE by a reactive load Z_{L1} to obtain $[S^{t3}]$ for the antennas and solve the equations of $S^{t3}_{21} = 0$ and $\mathrm{Re}\{Z_{L1}\} = 0$ for the phase delays $\boldsymbol{\theta}$ and reactive load Z_{L1}.

IV. Use the obtained $\boldsymbol{\theta}$ and Z_{L1} in Step III to obtain the input impedances of the decoupled antennas to design the matching circuits.

Since the design procedure is only based on $[S^{t1}]$ that can be obtained from simulation, this method should have no limitation on antenna configurations or types used in the system. Four benchmarks are used to demonstrate the superiorities of the proposed PDT as follows.

III. DECOUPLING EXAMPLES

In this section, four decoupling examples are presented and used to demonstrate the superiority of the proposed PDT. In these examples, the antennas are designed to operate at the center frequency of 2.40 GHz and implemented on the 0.8-mm Rogers RO4350 substrate with a relative permittivity of 3.66.

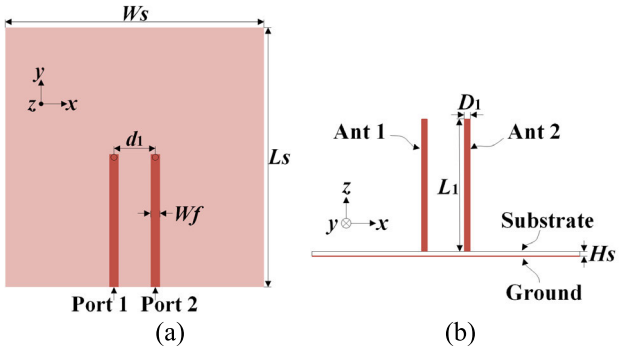

FIGURE 3. The coupled monopole array. (a) Top view. (b) Side view. (metal in front and metal in bottom.)

A. EXAMPLE 1: DECOUPLING OF TWO MONOPOLE ANTENNAS

A symmetric coupled array with two monopole antennas, denoted as Ant 1 and Ant 2, is shown in Fig. 3. The antennas have the same lengths $L_1 = 31$ mm and diameters $D_1 = 1.2$ mm. The center-to-center distance (antenna separation) is $d_1 = 8$ mm $= 0.06\lambda_0$. Both antennas are microstrip-fed on a substrate with the size of $Ls \times Ws = 50 \times 50$ mm^2 for good impedance matching. Nevertheless, the small separation certainly leads to poor antenna isolation. To increase isolation, the decoupling procedures proceed in detail as follows.

I. Add a PE with the same size as the antennas, in between Ants 1 and 2. The scattering matrix $[S^{t1}]$ of the three-port network at 2.4 GHz is obtained using CST simulation as

$$\mathbf{S^{t_1}} = \begin{bmatrix} 0.43\mathrm{e}^{-j1.80} & 0.42\mathrm{e}^{j1.36} & 0.51\mathrm{e}^{-j2.50} \\ 0.42\mathrm{e}^{j1.36} & 0.43\mathrm{e}^{-j1.80} & 0.51\mathrm{e}^{-j2.50} \\ 0.51\mathrm{e}^{-j2.50} & 0.51\mathrm{e}^{-j2.50} & 0.48\mathrm{e}^{-j4.00} \end{bmatrix} \tag{12}$$

Notably, in the proposed PDT, the PE operates as a parasitic scatterer for decoupling purposes. Hence, two factors are

$$\mathbf{S^{t_2}} = \begin{bmatrix} \alpha_{A1A1} e^{j(\phi_{A1A1} - 2\theta_1)} & \alpha_{A1A2} e^{j(\phi_{A1A2} - \theta_1 - \theta_2)} & \alpha_{A1P1} e^{j(\phi_{A1P1} - \theta_1 - \theta_3)} \\ \alpha_{A2A1} e^{j(\phi_{A2A1} - \theta_2 - \theta_1)} & \alpha_{A2A2} e^{j(\phi_{A2A2} - 2\theta_2)} & \alpha_{A2P1} e^{j(\phi_{A2P1} - \theta_2 - \theta_3)} \\ \alpha_{P1A1} e^{j(\phi_{P1A1} - \theta_3 - \theta_1)} & \alpha_{P1A2} e^{j(\phi_{P1A2} - \theta_3 - \theta_2)} & \alpha_{P1P1} e^{j(\phi_{P1P1} - 2\theta_3)} \end{bmatrix}. \tag{2}$$

essential when designing PE. Firstly, the resonant frequency of the PE should be close to that of antennas. Secondly, the PE should be placed in the near-field area of the antennas, so the antennas and PE could have a mutual coupling, i.e., $Z_{A1P1}^{t_1} \neq 0$ and $Z_{A2P1}^{t_1} \neq 0$. Under these two conditions, it is possible to manipulate and mitigate the mutual coupling ($S_{21}^{t_3}$) using the proposed PDT with appropriate reactive load (Z_{L1}) and phase delays (θ).

II. Add three meandering microstrip lines to the feed lines of the antennas and PE to introduce extra phase delays. Thus, the scattering matrix $[S^{t2}]$ for the system can be described by (13), as shown at the bottom of the next page. where $\{\theta_i \in \boldsymbol{\theta}, i \in [`1, 3]\}$ are generated from the added meandering microstrip-lines. Note that $S_{12}^{t_2} = S_{21}^{t_2}, S_{13}^{t_2} = S_{31}^{t_2}$ and $S_{23}^{t_2} = S_{32}^{t_2}$, due to reciprocity.

III. Terminate the PE by a reactive load Z_{L1}. For eliminating the mutual decoupling, with using the relevant Eqns. (3)-(9a), the variable Z_{L1} can be expressed by $[S^{t2}]$ as

$$Z_{L1} = Z_0 \left(S_{13}^{t_2} S_{23}^{t_2} - S_{12}^{t_2} - S_{12}^{t_2} S_{33}^{t_2}\right) / \left(S_{13}^{t_2} S_{23}^{t_2} + S_{12}^{t_2} - S_{12}^{t_2} S_{33}^{t_2}\right) \tag{14}$$

Due to the symmetrical layout of the system, $S_{13}^{t_2} = S_{23}^{t_2}$ in (14) yields the variable Z_{L1} as

$$Z_{L1} = Z_0 \left(\left(S_{13}^{t_2}\right)^2 - S_{12}^{t_2} - S_{12}^{t_2} S_{33}^{t_2}\right) / \left(\left(S_{13}^{t_2}\right)^2 + S_{12}^{t_2} - S_{12}^{t_2} S_{33}^{t_2}\right) \tag{15}$$

Substitute $[S^{t2}]$ in (13) into (15) to obtain Z_{L1} in terms of $\boldsymbol{\theta}$. Force $\mathrm{Re}\{Z_{L1}\} = 0$ using (10), a feasible solution of the phase delay is calculated as $\boldsymbol{\theta} = \{\theta_1, \theta_2, \theta_3\} = \{1.46, 1.46, 0.38\}$. The determined $\boldsymbol{\theta}$ is substituted in (16) to produce the reactance

$$Z_{L1} = \mathrm{Im}\{Z_{L1}\} = -j27.63\ (\Omega)$$

for the PE load. The reactance Z_{L1} is realized by a 2.4-pF capacitor.

IV. The input impedance of antennas after decoupling can be calculated by substituting $\boldsymbol{\theta}$ in (11) as

$$Z_{A1A1}^{t_3} = Z_{A2A2}^{t_3} = (8.88 - j52.36)\ \Omega$$

For illustration, the L-section matching network, consisting of a series 5.8-nH inductor and a shunt 1.5-pF capacitor, is adopted to transform the impedance ($Z_{A1A1}^{t_3}/Z_{A2A2}^{t_3}$) to 50-Ω matching at 2.4 GHz.

The complete decoupled array using the PDT is presented in Fig. 4. The bends of the added meandering microstrip lines are not mitered or curved since they have little effect on the antenna performance. Two fabrication samples of the coupled (w/o PDT) and decoupled (with PDT) arrays are presented in Fig. 5. The edge-launch SMA connectors for 0.8-mm slim PCBs are soldered to the antenna inputs for feeding. The vector network analyzer Rohde & Schwarz ZVA 24 is employed to measure the S-parameters of the antenna prototype, and the antenna measurement system, the Satimo StarLab [30], is used to measure its radiation pattern and efficiency.

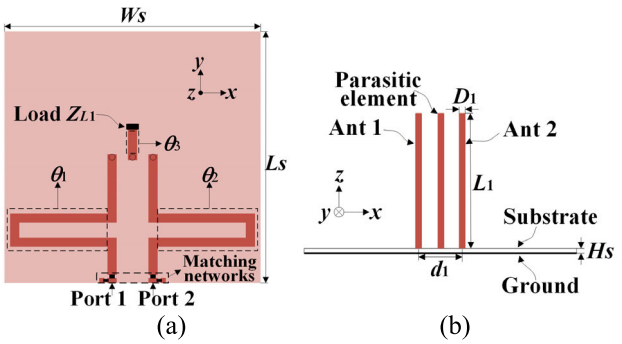

FIGURE 4. The decoupled monopole array. (a) Top view. (b) Side view. (metal in front and metal in bottom.)

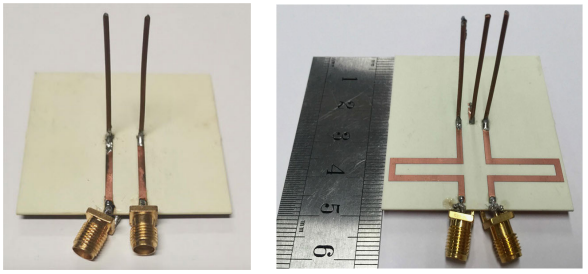

FIGURE 5. Prototyped antennas. (a) The coupled monopole array. (b) The decoupled array.

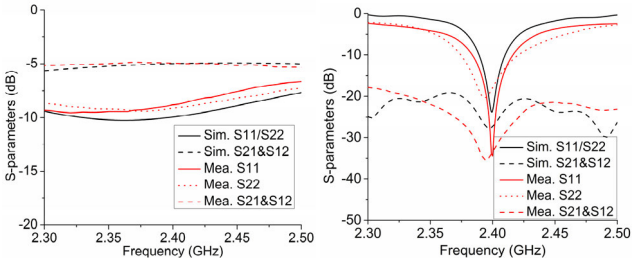

FIGURE 6. Simulated and measured S-parameters. (a) The coupled monopole array. (b) The decoupled array.

Fig. 6(a) shows the simulated and measured S-parameters of the coupled array. It can be seen that the port isolation, as indicated by S_{21}, as well as the reflection coefficient for each antenna port, as indicated by S_{11}/S_{22}, are both poor due to the small antenna separation of $0.06\lambda_0$. The isolation is only ∼5 dB at 2.4 GHz. The S-parameters of the decoupled array are shown in Fig. 6(b). The comparison of Figs. 6(a) and 6(b) demonstrate that the simulated isolation after decoupling is increased from 5 dB to 27 dB. It is also seen from Fig. 6(b) that the measured impedance bandwidth (IMBW) with $S_{11}\&S_{22} < -10$ dB is from 2.38 to 2.42 GHz (1.66%), indicating the improved reflection coefficient for each port after decoupling. Besides, the narrowband issue is caused by the very limited antenna separation (d_1) and the adoption of the L-section narrowband matching circuit.

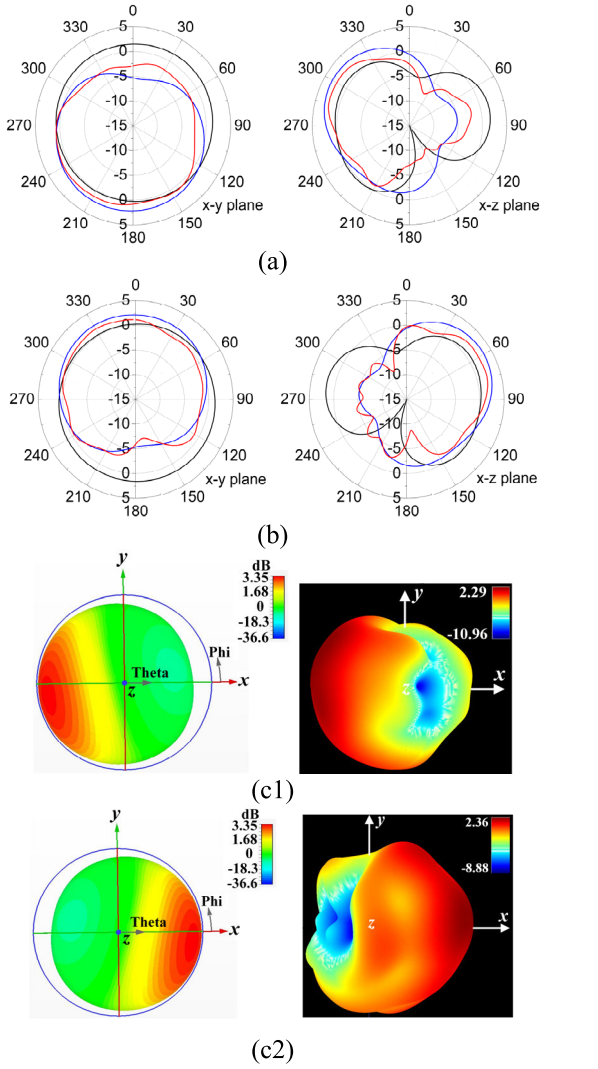

FIGURE 7. Simulated and measured radiation patterns with (a) port 1 and (b) port 2 excited. (——— Sim. Coupled, ——— Sim. Decoupled, and ——— Mea. Decoupled) and (c) 3-D radiation patterns for (c1) port 1 or (c2) port 2 excited.

The radiation patterns of the coupled and decoupled array are shown in Fig. 7. The 3-D radiation patterns are shown in Fig. 7(c) for better comparison. It can be seen that the patterns of two antennas are symmetric to each other with respect to the y-z plane. The coupled antenna performs the omnidirectional patterns in the x-y plane, which is similar to that of a conventional monopole antenna. After using the proposed PDT, the radiation pattern becomes directional. It indicates that the proposed PDT leads to the improved pattern diversity with two complementary patterns when two antennas are fed separately, which is thus suitable for the application in MIMO systems with multiple signal paths.

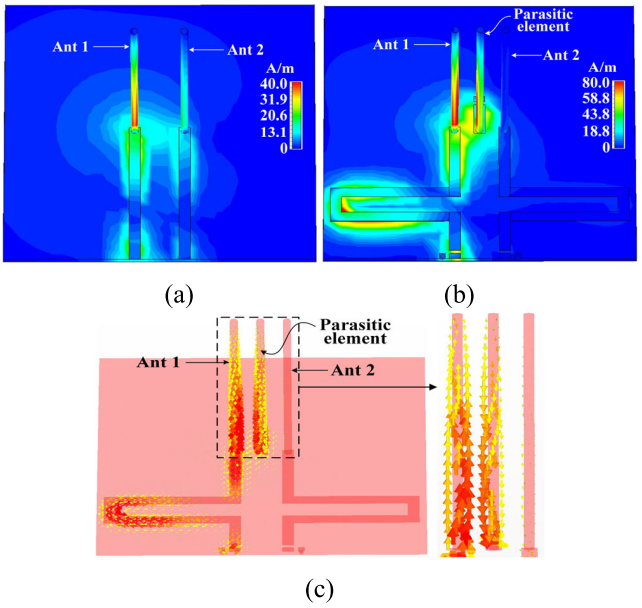

FIGURE 8. Simulated current distributions. (a) Coupled array. (b) & (c): Decoupled array using the PDT.

To further reveal the parasitic decoupling mechanism, the simulated current distributions of the coupled and decoupled monopole arrays at 2.4 GHz are presented in Fig. 8. As shown in Fig. 8(a), for the coupled antennas, when port 1 is excited, both Ant 1 and Ant 2 show strong current distributions. After using the proposed PDT, as shown in Figs. 8(b) and 8(c), when port 1 is driven, strong currents are distributed along with Ant 1 and the PE, while Ant 2 is with little current distribution. Moreover, Fig. 8(c) shows around the 180°-phase difference between the excited antenna (Ant 1) and the PE, generating an out-of-phase far-field cancellation and leading to the patterns pointed to the $-x$-direction, as shown in Fig. 8(c1).

The 180°-phase difference is a combining result of the distance (between the antenna and PE) and the reactive load for the PE. When the distance, corresponding to a wave-propagation delay and causing a phase difference, is fixed, the value of reactive load Z_{L1} is appropriately determined by the proposed methodology to achieve around 180°-phase difference. As a result, the interference from the excited antenna (Ant 1) and PE will cancel out the original antenna coupling for isolation enhancement.

Fig. 9(a) shows the total efficiency before and after decoupling. It can be observed that the simulated efficiencies before and after decoupling are 56%-58% and 72%-91%, respectively, demonstrating an enhancement of around 16%-33% after using the proposed PDT. The increasement of total efficiency is caused by improvements in isolation and

$$\mathbf{S}^{\mathbf{t_2}} = \begin{bmatrix} 0.43e^{-j(1.80+2\theta_1)} & 0.42e^{j(1.36-\theta_1-\theta_2)} & 0.51e^{-j(2.50+\theta_1+\theta_3)} \\ 0.42e^{j(1.36-\theta_2-\theta_1)} & 0.43e^{-j(1.80+2\theta_2)} & 0.51e^{-j(2.50+\theta_2+\theta_3)} \\ 0.51e^{-j(2.50+\theta_3+\theta_1)} & 0.51e^{-j(2.50+\theta_3+\theta_2)} & 0.48e^{-j(4.00+2\theta_3)} \end{bmatrix} \tag{13}$$

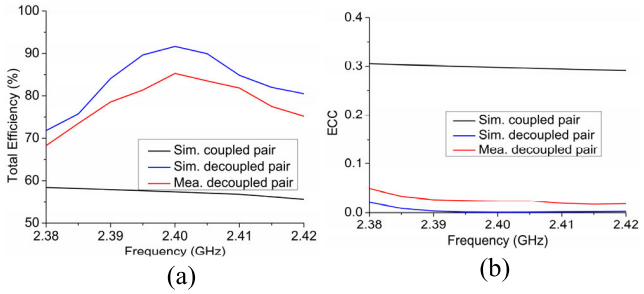

FIGURE 9. Simulated and measured (a) total efficiencies and (b) ECCs of the monopole array.

impedance matching. Besides, the measured efficiencies of the decoupled array are 68%-85%. The discrepancy between the simulated and measured results is caused by the cable effect [31]. The cable effect on small antenna measurement has been studied in [31] in detail and is not shown here to save space.

It is known that envelope correlation coefficients (ECC) ρ_e is an important figure of merit for MIMO antennas. A lower ECC reflects a low correlation of two antennas. It is calculated by the complex far-field radiation patterns as [32]

$$\rho_e \approx |\rho_c|^2 \tag{16}$$

where ρ_c is the complex correlation coefficient given by

$$\rho_c = \int_0^{2\pi} M_{12}(\phi)d\phi \Big/ \sqrt{\int_0^{2\pi} M_{11}(\phi)d\phi \int_0^{2\pi} M_{22}(\phi)d\phi} \tag{17}$$

$$M_{ij}(\phi) = \Gamma E_{\theta i}(\pi/2, \phi)E^*_{\theta j}(\pi/2, \phi) + E_{\phi i}(\pi/2, \phi)E^*_{\phi j}(\pi/2, \phi) \tag{18}$$

The ECCs within the IMBW of 2.38-2.42 GHz are calculated by (17) and (18). Fig. 9(b) shows that the ECCs of the coupled monopole array using the simulated patterns are around 0.3. The ECCs of the decoupled array using simulated patterns are improved to around zero value, and the measured ECC is below 0.05. The results reveal that the decoupled array can achieve a better diversity performance since a MIMO system with lower ECC achieves higher diversity gain [32].

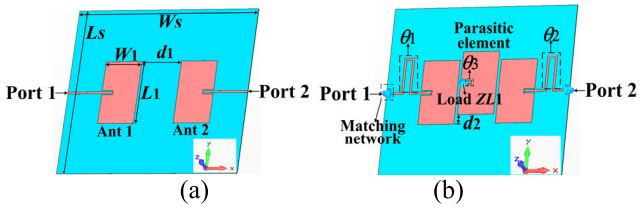

FIGURE 10. (a) The coupled patch array. (b) The decoupled array.

B. EXAMPLE 2: DECOUPLING OF TWO PATCH ANTENNAS

To demonstrate that the proposed PDT has no limitation on antenna type or configuration, a pair of patch antennas are considered in this example. Fig. 10(a) shows a two-element antenna array having two coupled patches, denoted as Ants 1 and 2, with the same lengths $L_1 = 56$ mm and widths $W_1 = 31.6$ mm. The antenna separation is $d_1 = 34.8$ mm $= 0.27\lambda_0$. Both antennas are microstrip-fed on a substrate with a size of $Ls \times Ws = 150 \times 158$ mm^2 for good impedance matching. The decoupled array is shown in Fig. 10(b). A PE with the same size as the patches is inserted in between the antennas for decoupling purposes. The position of the PE is equidistant from the two antennas, but not exactly in between them. The off-center distance is $d_2 = 8$ mm, as shown in Fig. 10(b). It indicates that the proposed PDT is still effective if the PE is not exactly placed in the middle of the antennas.

Following the decoupling procedure in example 1, the phase delays and load are calculated as $\{\theta_1, \theta_2, \theta_3\} = \{4.59, 4.59, 0.57\}$ and $Z_{L1} = -j44.21$, respectively. Then, Z_{L1} is realized by a 1.5-pF capacitor at 2.4 GHz. The L-section matching network, consisting of a series 2.5-nH inductor and a shunt 2.0-pF capacitor, is used at each antenna input.

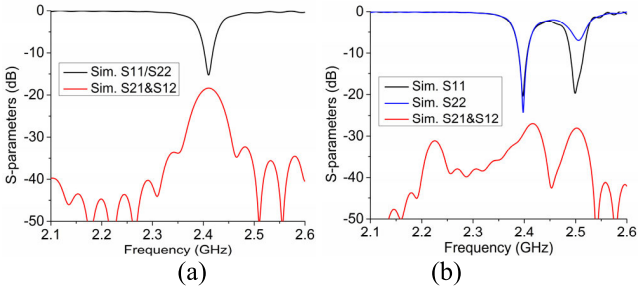

FIGURE 11. Simulated S-parameters. (a) The original and (b) the decoupled patch arrays.

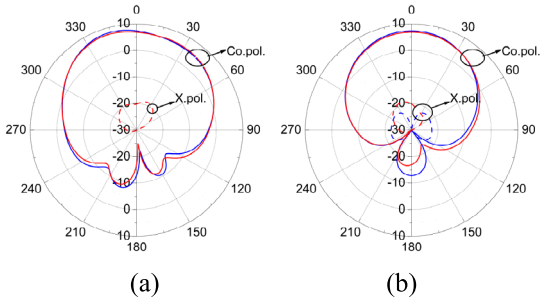

FIGURE 12. Simulated radiation patterns of the coupled and decoupled patch arrays with port 1 excited. (a) x-z plane (E-plane). (b) y-z plane (H-plane). (——— Coupled and ——— Decoupled).

The simulated S-parameters of the patch array are shown in Fig. 11. Fig. 11(a) shows that the simulated isolation of the coupled antennas is around 18 dB at 2.4 GHz. The comparison of Figs. 11(a) and 11(b) demonstrate that isolation is increased from 18 to 29 dB. The simulated radiation patterns are shown in Fig. 12. The patterns before and after decoupling are nearly the same. The results of total efficiency and ECC are shown in Fig. 13. It can be seen that after

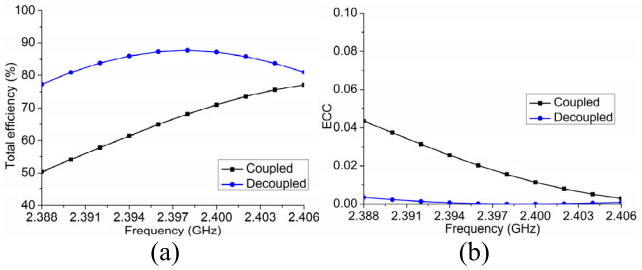

FIGURE 13. Simulated (a) total efficiency and (b) ECC of the patch array.

adopting the proposed PDT, the efficiency is improved and the ECC is reduced.

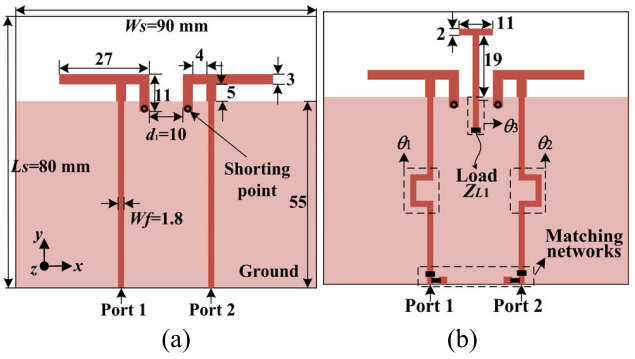

FIGURE 14. (a) The coupled IFA array. (b) The decoupled array.

C. EXAMPLE 3: DECOUPLING OF TWO IFA ANTENNAS

To further demonstrate that the proposed PDT suits for most MIMO antennas and to demonstrate that the PE can be different antenna types from the excited antennas, the PDT is applied for decoupling a two-element inverted-F antenna (IFA) array in this example. Fig. 14(a) shows two coupled IFAs with the edge separation distance $d_1 = 10$ mm. A metallic pin with a 0.8-mm radius is implemented to connect the IFA's shorting arm to the ground. Both antennas are microstrip-fed on an 80 mm×90 mm substrate for impedance matching.

Fig. 14(b) shows the final array after adopting the proposed PDT. A T-shaped monopole, acting as the PS, is inserted in between the IFAs for isolation enhancement. Following the decoupling procedures in example 1, the TL-length parameters are calculated to be $\theta_1 = \theta_2 = 1.53$ and $\theta_3 = 1.15$. The load reactance Z_{L1} is calculated to be $-j132.60\ \Omega$, which is then realized by a 0.5-pF capacitor. For matching purposes, the L-section matching circuit, consisting of a series 3.4-nH inductor and a shunt 0.9-pF capacitor, is used at each antenna input.

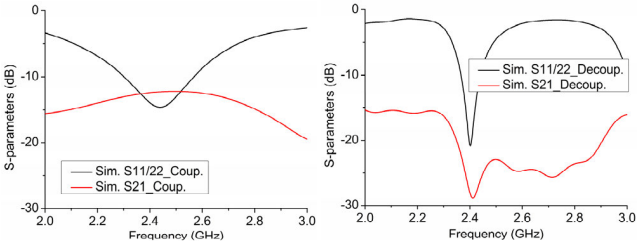

FIGURE 15. Simulated S-parameters of (a) the coupled and (b) the decoupled IFA arrays.

From the simulated S-parameters in Figs. 15(a) and 15(b), it can be seen that the isolation (S_{21}) between two IFAs are significantly improved from ∼13 dB to ∼28 dB by 15 dB after using the proposed PDT. The results verified the feasibility of utilizing PE in different antenna types in-between antennas for isolation enhancement. The results of efficiency and ECC are shown in Fig. 16, which demonstrates the improvement of efficiency and reduction of ECC by using the proposed PDT.

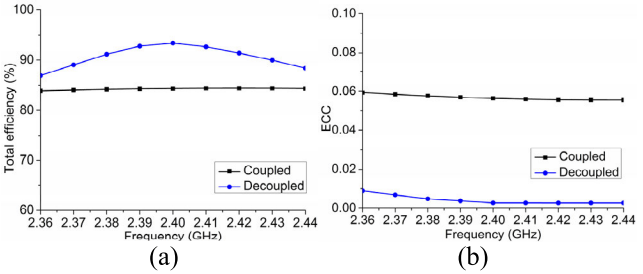

FIGURE 16. Simulated (a) total efficiency and (b) ECC of the IFA array.

D. EXAMPLE 4: DECOUPLING OF THREE MONOPOLE ANTENNAS

To demonstrate the potential of the proposed PDT for multiple-element MIMO antennas [33], an extension work of

$$\mathbf{Z}^{t_3} = \begin{bmatrix} Z^{t_2}_{A1A1} & Z^{t_2}_{A1A2} & Z^{t_2}_{A1A3} \\ Z^{t_2}_{A2A1} & Z^{t_2}_{A2A2} & Z^{t_2}_{A2A3} \\ Z^{t_2}_{A3A1} & Z^{t_2}_{A3A2} & Z^{t_2}_{A3A3} \end{bmatrix} - \begin{bmatrix} Z^{t_2}_{A1P1} & Z^{t_2}_{A1P2} & Z^{t_2}_{A1P3} \\ Z^{t_2}_{A2P1} & Z^{t_2}_{A2P2} & Z^{t_2}_{A2P3} \\ Z^{t_2}_{A3P1} & Z^{t_2}_{A3P2} & Z^{t_2}_{A3P3} \end{bmatrix} \begin{bmatrix} Z^{t_2}_{P1P1}+Z_{L1} & Z^{t_2}_{P1P2} & Z^{t_2}_{P1P3} \\ Z^{t_2}_{P2P1} & Z^{t_2}_{P2P2}+Z_{L2} & Z^{t_2}_{P2P3} \\ Z^{t_2}_{P3P1} & Z^{t_2}_{P3P2} & Z^{t_2}_{P3P3}+Z_{L3} \end{bmatrix}^{-1} \begin{bmatrix} Z^{t_2}_{P1A1} & Z^{t_2}_{P1A2} & Z^{t_2}_{P1A3} \\ Z^{t_2}_{P2A1} & Z^{t_2}_{P2A2} & Z^{t_2}_{P2A3} \\ Z^{t_2}_{P3A1} & Z^{t_2}_{P3A2} & Z^{t_2}_{P3A3} \end{bmatrix}$$
$$= \begin{bmatrix} f^{t_3}_{A1A1}(\mathbf{Z_L}, \boldsymbol{\theta}) & f^{t_3}_{A1A2}(\mathbf{Z_L}, \boldsymbol{\theta}) & f^{t_3}_{A1A3}(\mathbf{Z_L}, \boldsymbol{\theta}) \\ f^{t_3}_{A2A1}(\mathbf{Z_L}, \boldsymbol{\theta}) & f^{t_3}_{A2A2}(\mathbf{Z_L}, \boldsymbol{\theta}) & f^{t_3}_{A2A3}(\mathbf{Z_L}, \boldsymbol{\theta}) \\ f^{t_3}_{A3A1}(\mathbf{Z_L}, \boldsymbol{\theta}) & f^{t_3}_{A3A2}(\mathbf{Z_L}, \boldsymbol{\theta}) & f^{t_3}_{A3A3}(\mathbf{Z_L}, \boldsymbol{\theta}) \end{bmatrix} \quad (19)$$

applying the PDT for decoupling a three-element monopole array is conducted. Three monopole antennas, designed to operate at 2.4 GHz with the lengths of 29 mm (about $\lambda_0/4$) and diameters of 1.0 mm, are arranged into an isosceles-triangle array on a Rogers RO 4350 substrate with a size of 60×60 mm^2, as shown in Fig. 17(a). The antenna separations are $d_1 = 28$ mm $= 0.22\lambda_0$ and $d_2 = 18.5$ mm $= 0.15\lambda_0$. The final decoupled array using the proposed PDT is presented in Fig. 17(b).

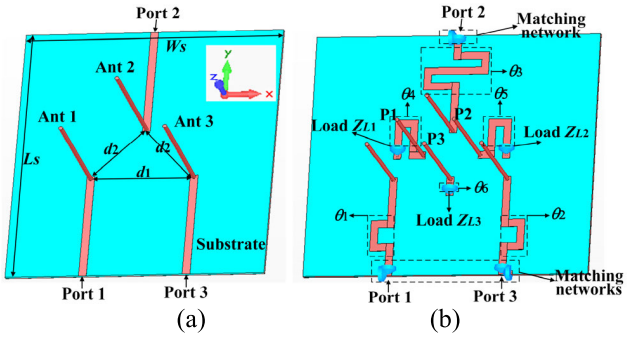

FIGURE 17. (a) The original three-element monopole array. (b) The decoupled array using the proposed PDT.

The designed PDS consists of six TLs ($\theta_1 - \theta_6$), three PEs (P1-P3), and three reactive loads ($Z_{L1} - Z_{L3}$), as shown in Fig. 15(b). Similar to deriving (7) for obtaining the antenna impedance at reference plane t_3, the corresponding expression for this case is given by (19), as shown at the bottom of the previous page. For eliminating the coupling among antennas, the following requirements should be satisfied simultaneously,

$$\begin{cases} Z_{21}^{t_3} = f_{A2A1}^{t_3}(\mathbf{Z_L}, \boldsymbol{\theta}) = 0 \\ Z_{31}^{t_3} = f_{A3A1}^{t_3}(\mathbf{Z_L}, \boldsymbol{\theta}) = 0 \\ Z_{32}^{t_3} = f_{A3A2}^{t_3}(\mathbf{Z_L}, \boldsymbol{\theta}) = 0. \end{cases} \tag{20}$$

In the same way, $\mathbf{Z_L}$ should be purely imaginary to avoid ohmic loss, i.e.,

$$\mathrm{Re}\{Z_{L1}\} = \mathrm{Re}\{Z_{L2}\} = \mathrm{Re}\{Z_{L3}\} = 0. \tag{21}$$

By solving Eqns. (20) and (21) simultaneously, the phase delays and loads are calculated as $\{\theta_1, \theta_2, \theta_3, \theta_4, \theta_5, \theta_6\} = \{0.71, 0.71, 2.15, 1.03, 1.03, 0.23\}$ and $\{Z_{L1}, Z_{L2}, Z_{L3}\} = \{j82.89, -j82.89, j13.57\}$, respectively. The reactive loads are realized by two capacitors (0.8 pF) and one inductor (0.9 nH).

The input impedances $\left\{Z_{ii}^{t_3} \in \mathbf{Z}^{t_3}, i \in [1, 3]\right\}$ of the decoupled antennas are calculated by (19) as

$$Z_{A1A1}^{t_3} = Z_{A2A2}^{t_3} = (12.09 - j9.70)\ \Omega$$
$$Z_{A3A3}^{t_3} = (13.50 + j67.39)\ \Omega$$

Three L-section matching circuits, consisting of a series inductor (2.9 nH) with a shunt capacitor (2.0 pF) for port 1/2 and a series capacitor (1.6 pF) with a shunt capacitor (2.1 pF) for port 3, are individually implemented at each antenna input.

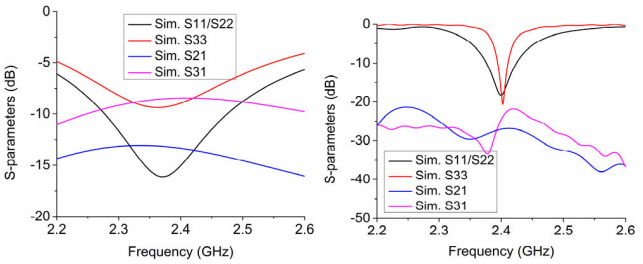

FIGURE 18. Simulated S-parameters of (a) the coupled and (b) the decoupled three-element monopole arrays.

The simulated S-parameters of the three-element array are shown in Fig. 18. Note that $S_{31} = S_{32}$, due to the symmetric layout. It can be seen from Fig. 18(a) that without using the PDT, the couplings between Ants 1&2 and 1&3 at 2.4 GHz are -13 and -8 dB, respectively. After using the proposed PDT, S_{21} and S_{31} are substantially reduced to -28 and -24 dB, respectively, at 2.4 GHz. The results indicate that the proposed PDT has the potential of decoupling multiple-element MIMO antennas. The results of total efficiency and ECC are shown in Fig. 19. It shows that after adopting the proposed PDT, the efficiency is improved and the ECC is reduced.

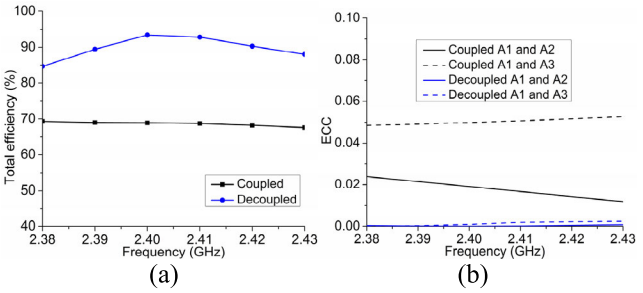

FIGURE 19. Simulated (a) total efficiency and (b) ECC of the three-monopole array.

E. COMPARISON WITH OTHER DECOUPLING WORKS

The proposed PDT is compared with some alternative decoupling solutions in terms of isolation bandwidth (BW), total efficiency, structural complexity, etc. The comparison results are summarized as follows.

1) COMPARED WITH OTHER PDTs

The PDTs in [26], [27] utilized a reactively loaded PE to increase isolation. High isolation and efficiency, as well as narrow BW, were achieved. In comparison, the proposed PDT provides a similar isolation level and BW, but in a more accurate realization since no parametrical optimization is required.

2) COMPARED WITH DFNs

The DFN in [4] utilized additional TLs to obtain the imaginary trans-admittance that was then canceled by a shunt component. It achieved a similar BW with the proposed PDT. Besides, the proposed PDT provided a similar isolation level and bandwidth as [13], and showed the superior on applicability to more antennas. Recently, authors in [10]–[12] replaced the reactive component in [4] by a coupled-resonator decoupling network (CRDN), which could achieve a wider BW at the expense of more complicated network realization. Hence, inspired by the CRDN, we expect that if the Q-factor of the proposed PDT is reduced through replacing the reactive component (Z_{L1}) by an LC circuit, a wider isolation BW could be achieved.

IV. CONCLUSION

This paper presented a PDT for two antennas. The main intention of this paper is to provide a theoretical insight into this approach, which can be applied to other configurations and types of antennas used in MIMO systems. The detailed decoupling theory and design procedure were illustrated by four decoupling examples. The simulated and measured results showed that isolations over 24 dB, efficiencies above 70%, and envelop correlation coefficients below 0.05 were achieved. Besides, the proposed PDS results in diversity radiation patterns when antennas are fed separately, which is explained by the simulated surface current distribution. Moreover, we expect that the proposed PDT has the potential for multiple-element MIMO antennas.

REFERENCES

[1] A. Chebihi, C. Luxey, A. Diallo, P. Le Thuc, and R. Staraj, "A novel isolation technique for closely spaced PIFAs for UMTS mobile phones," *IEEE Antennas Wireless Propag. Lett.*, vol. 7, pp. 665–668, 2008.
[2] A. Diallo, C. Luxey, P. Le Thuc, R. Staraj, and G. Kossiavas, "Study and reduction of the mutual coupling between two mobile phone PIFAs operating in the DCS1800 and UMTS bands," *IEEE Trans. Antennas Propag.*, vol. 54, no. 11, pp. 3063–3074, Nov. 2006.
[3] X. Ling and R. Li, "A novel dual-band MIMO antenna array with low mutual coupling for portable wireless devices," *IEEE Antennas Wireless Propag. Lett.*, vol. 10, pp. 1039–1042, 2011.
[4] S.-C. Chen, Y.-S. Wang, and S.-J. Chung, "A decoupling technique for increasing the port isolation between two strongly coupled antennas," *IEEE Trans. Antennas Propag.*, vol. 56, no. 12, pp. 3650–3658, Dec. 2008.
[5] R.-L. Xia, S.-W. Qu, P.-F. Li, Q. Jiang, and Z.-P. Nie, "An efficient decoupling feeding network for microstrip antenna array," *IEEE Antennas Wireless Propag. Lett.*, vol. 14, pp. 871–874, 2015.
[6] K.-C. Lin, C.-H. Wu, C.-H. Lai, and T.-G. Ma, "Novel dual-band decoupling network for two-element closely spaced array using synthesized microstrip lines," *IEEE Trans. Antennas Propag.*, vol. 60, no. 11, pp. 5118–5128, Nov. 2012.
[7] C.-H. Wu, C.-L. Chiu, and T.-G. Ma, "Very compact fully lumped decoupling network for a coupled two-element array," *IEEE Antennas Wireless Propag. Lett.*, vol. 15, pp. 158–161, 2016.
[8] X. Tang, K. Mouthaan, and J. C. Coetzee, "Tunable decoupling and matching network for diversity enhancement of closely spaced antennas," *IEEE Antennas Wireless Propag. Lett.*, vol. 11, pp. 268–271, 2012.
[9] X. Tang, X. Qing, and Z. N. Chen, "Simplification and implementation of decoupling and matching network with port pattern-shaping capability for two closely spaced antennas," *IEEE Trans. Antennas Propag.*, vol. 63, no. 8, pp. 3695–3699, Aug. 2015.
[10] L. Zhao, L. K. Yeung, and K.-L. Wu, "A coupled resonator decoupling network for two-element compact antenna arrays in mobile terminals," *IEEE Trans. Antennas Propag.*, vol. 62, no. 5, pp. 2767–2776, May 2014.
[11] L. Zhao and K.-L. Wu, "A dual-band coupled resonator decoupling network for two coupled antennas," *IEEE Trans. Antennas Propag.*, vol. 63, no. 7, pp. 2843–2850, Jul. 2015.
[12] K. Qian, L. Zhao, and K.-L. Wu, "An LTCC coupled resonator decoupling network for two antennas," *IEEE Trans. Microw. Theory Techn.*, vol. 63, no. 10, pp. 3199–3207, Oct. 2015.
[13] M. Li, L. Jiang, and K. L. Yeung, "Novel and efficient parasitic decoupling network for closely coupled antennas," *IEEE Trans. Antennas Propag.*, vol. 67, no. 6, pp. 3574–3585, Jun. 2019.
[14] H.-P. Li, G.-M. Wang, T. Cai, J.-G. Liang, and X.-J. Gao, "Phase- and amplitude-control metasurfaces for antenna main-lobe and sidelobe manipulations," *IEEE Trans. Antennas Propag.*, vol. 66, no. 10, pp. 5121–5129, Oct. 2018.
[15] H. Li, G. Wang, T. Cai, H. Hou, and W. Guo, "Wideband transparent beamforming metadevice with amplitude- and phase-controlled metasurface," *Phys. Rev. A, Gen. Phys. Appl.*, vol. 11, no. 1, Jan. 2019, Art. no. 014043.
[16] H. Li, G. Wang, T. Cai, J. Liang, and H. Hou, "Bifunctional circularly-polarized lenses with simultaneous geometrical and propagating phase control metasurfaces," *J. Phys. D, Appl. Phys.*, vol. 52, no. 46, Nov. 2019, Art. no. 465105.
[17] F. Yang and Y. Rahmat-Samii, "Microstrip antennas integrated with electromagnetic band-gap (EBG) structures: A low mutual coupling design for array applications," *IEEE Trans. Antennas Propag.*, vol. 51, no. 10, pp. 2936–2946, Oct. 2003.
[18] H. S. Farahani, M. Veysi, M. Kamyab, and A. Tadjalli, "Mutual coupling reduction in patch antenna arrays using a UC-EBG superstrate," *IEEE Antennas Wireless Propag. Lett.*, vol. 9, pp. 57–59, 2010.
[19] A. Habashi, J. Nourinia, and C. Ghobadi, "Mutual coupling reduction between very closely spaced patch antennas using low-profile folded split-ring resonators (FSRRs)," *IEEE Antennas Wireless Propag. Lett.*, vol. 10, pp. 862–865, 2011.
[20] Z. Qamar, L. Riaz, S. A. Khan, M. Chongcheawchamnan, and M. F. Shafique, "Slot combined complementary split ring resonators for mutual coupling suppression in microstrip phased arrays," *IET Microw., Antennas Propag.*, vol. 8, no. 15, pp. 1261–1267, Dec. 2014.
[21] Z. Qamar, U. Naeem, S. A. Khan, M. Chongcheawchamnan, and M. F. Shafique, "Mutual coupling reduction for high-performance densely packed patch antenna arrays on finite substrate," *IEEE Trans. Antennas Propag.*, vol. 64, no. 5, pp. 1653–1660, May 2016.
[22] A. C. K. Mak, C. R. Rowell, and R. D. Murch, "Isolation enhancement between two closely packed antennas," *IEEE Trans. Antennas Propag.*, vol. 56, no. 11, pp. 3411–3419, Nov. 2008.
[23] S. Farsi, H. Aliakbarian, D. Schreurs, B. Nauwelaers, and G. A. E. Vandenbosch, "Mutual coupling reduction between planar antennas by using a simple microstrip U-section," *IEEE Antennas Wireless Propag. Lett.*, vol. 11, pp. 1501–1503, 2012.
[24] S. Soltani and R. D. Murch, "A compact planar printed MIMO antenna design," *IEEE Trans. Antennas Propag.*, vol. 63, no. 3, pp. 1140–1149, Mar. 2015.
[25] K.-L. Wu, C. Wei, X. Mei, and Z.-Y. Zhang, "Array-antenna decoupling surface," *IEEE Trans. Antennas Propag.*, vol. 65, no. 12, pp. 6728–6738, Dec. 2017.
[26] B. K. Lau and J. B. Andersen, "Simple and efficient decoupling of compact arrays with parasitic scatterers," *IEEE Trans. Antennas Propag.*, vol. 60, no. 2, pp. 464–472, Feb. 2012.
[27] L. Zhao and K.-L. Wu, "A decoupling technique for four-element symmetric arrays with reactively loaded dummy elements," *IEEE Trans. Antennas Propag.*, vol. 62, no. 8, pp. 4416–4421, Aug. 2014.
[28] D. M. Pozar, *Microwave Engineering*, 3rd ed. New York, NY, USA: Wiley, 2005.
[29] R. Vaughan and J. A. Bach, *Channels, Propagation and Antennas for Mobile Communications*. London, U.K.: The IEEE, 2003, p. 511.
[30] The Microwave Vision Group, Paris, France. (2018). *The Satimo Starlab System*. [Online]. Available: http://www.satimo.com/
[31] L. Liu, S. W. Cheung, and T. I. Yuk, "Compact MIMO antenna for portable devices in UWB applications," *IEEE Trans. Antennas Propag.*, vol. 61, no. 8, pp. 4257–4264, Aug. 2013.
[32] R. G. Vaughan and J. B. Andersen, "Antenna diversity in mobile communications," *IEEE Trans. Veh. Technol.*, vol. 36, no. 4, pp. 149–172, Nov. 1987.
[33] X.-J. Zou, G.-M. Wang, Y.-W. Wang, and H.-P. Li, "An efficient decoupling network between feeding points for multielement linear arrays," *IEEE Trans. Antennas Propag.*, vol. 67, no. 5, pp. 3101–3108, May 2019.

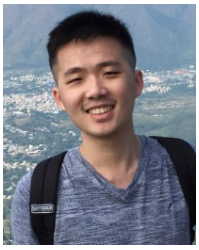

MIN LI (Member, IEEE) received the B.S. degree from UESTC, Chengdu, China, in 2014, and the Ph.D. degree from The University of Hong Kong, Hong Kong, in 2018. He is currently a Postdoctoral Researcher with the Department of Electrical and Electronic Engineering, The University of Hong Kong. His current research interests include antenna design and multiple-input multiple-output antenna decoupling.

DI WU (Member, IEEE) received the B.Eng. degree in electromagnetic field and microwave technology from the University of Electronic Science and Technology of China (UESTC), Chengdu, China, in 2009, the M.S. degree from the City University of Hong Kong, Hong Kong, in 2013, and the Ph.D. degree from The University of Hong Kong, Hong Kong, in 2018.

From 2010 to 2012, he was with MediaTek.Inc. (MTK), as a Senior RF Engineer. In 2017, he was a Visiting Ph.D. with the University of Wisconsin-Madison, Madison, WI, USA. From 2018 to 2019, he was with the Hong Kong Applied Science and Technology Research Institute (ASTRI), Hong Kong, as a Senior System Design Engineer. Since January 2019, he has been with the College of Electronic Science and Technology, Shenzhen University, Shenzhen, China, as an Assistant Professor. His current research interests include phased array systems, phase shifter, antennas, and RF/microwave circuits.

BING XIAO (Student Member, IEEE) received the B.Sc. degree in applied physics from Anhui University, Hefei, China, in 2009, the M.Sc. degree in radio physics from the University of Electronic Science and Technology of China (UESTC), Chengdu, China, in 2012. He is currently pursuing the Ph.D. degree in electronic engineering with The University of Hong Kong, Hong Kong. He was an Antenna/RF Engineer with China Electronics Technology Group Corporation (CETC), in 2012. He was also with Xiaomi Corporation. His current research interests include smart devices and the IoT antennas.

KWAN LAWRENCE YEUNG (Senior Member, IEEE) was born in 1969. He received the B.Eng. and Ph.D. degrees in information engineering from The Chinese University of Hong Kong, in 1992 and 1995, respectively. He joined the Department of Electrical and Electronic Engineering, The University of Hong Kong, in July 2000, where he is currently a Professor. His research interests include next-generation internet, packet switch/router design, all-optical networks, and wireless data networks.

LIJUN JIANG (Fellow, IEEE) received the B.S. degree in electrical engineering from the Beijing University of Aeronautics and Astronautics, Beijing, China, in 1993, the M.S. degree from Tsinghua University, Beijing, in 1996, and the Ph.D. degree from the University of Illinois at Urbana–Champaign, Champaign, IL, USA, in 2004. From 1996 to 1999, he was an Application Engineer with Hewlett-Packard Company. Since 2004, he has been a Postdoctoral Researcher, a Research Staff Member, and a Senior Engineer with the IBM T. J. Watson Research Center, Yorktown Heights, NY, USA. Since 2009, he has been an Associate Professor with the Department of Electrical and Electronic Engineering, The University of Hong Kong, Hong Kong. He was a Scientific Consultant with Hong Kong Applied Science and Technology Research Institute Company Ltd., from 2010 to 2011. Since 2013, he has been a Senior Visiting Professor with Tsinghua University. He has been a Panellist on the Expert Review Panel with the Hong Kong Research and Development Center for Logistics and Supply Chain Management Enabling Technologies, since 2013. He was with Semiconductor Research Cooperation (SRC) Industrial Liaison for several academic projects. He has been involved collaboratively with many international researchers. He is a member of the IEEE AP-S, the IEEE MTT-S, the IEEE EMC-S, an ACES, and the Chinese Computational Electromagnetics Society. He has been an Elected TPC Member of the IEEE Electrical Design of Advanced Packaging and Systems Symposium (EDAPS), since 2010. He has been a TC-9 Member and a TC-10 Member of the IEEE Electromagnetic Compatibility Society, since 2011. He was a Scientific Committee Member of the 2010 IEEE Simulation and Modeling of Emerging Electronics, the Special Session Organizer of the IEEE EDAPS, the IEEE Electromagnetic Compatibility Society, the Applied Computational Electromagnetics Society, the Asia-Pacific Radio Science Conference, and the Progress in Electromagnetics Research Symposium, and a Co-Organizer of the HKU Computational Science and Engineering Workshops, from 2010 to 2012. He was a TPC Member of the 2013 IEEE International Conference on Microwave Technology and Computational Electromagnetics. He also has been an Elected TPC Member of the IEEE Electrical Performance of Electronic Packaging, since 2014. He received the IEEE MTT Graduate Fellowship Award, in 2003, and the Y. T. Lo Outstanding Research Award, in 2004. He was the Session Chair of many international conferences. He was a TPC Chair of the seventh International Conference on Nanophotonics/third Conference on Advances in Optoelectronics and Micro/Nano Optics, a TPC Co-Chair of the 12th International Workshop on Finite Elements for Microwave Engineering, the 2013 International Workshop on Pulsed Electromagnetic Field at Delft, The Netherlands, and the General Chair of the 2014 IEEE 14th HK AP/MTT Postgraduate Conference. He serves as an Associate Guest Editor for the Proceedings of the IEEE Special Issue, from 2011 to 2012. He serves as an Associate Editor for the IEEE TRANSACTIONS ON ANTENNAS AND PROPAGATION and *Progress in Electromagnetics Research*. He also serves as a Reviewer for the IEEE TRANSACTIONS on several topics and other primary electromagnetics and microwave related journals.